On the Kinetics of Adsorption and Two-Dimensional Self-Assembly of Annexin A5 on Supported Lipid Bilayers

Ralf P. Richter, Joséphine Lai Kee Him, Béatrice Tessier, Céline Tessier, and Alain R. Brisson
Laboratoire d'Imagerie Moléculaire et NanoBioTechnologie, IECB, UMR-CNRS 5471, Université Bordeaux 1, 33607 Pessac Cedex, France

ABSTRACT Annexin A5 is a protein that binds to membranes containing negatively charged phospholipids in a calcium-dependent manner. We previously found that annexin A5 self-assembles into two-dimensional (2D) crystals on supported lipid bilayers (SLBs) formed on mica while a monolayer of disordered trimers is formed on SLBs on silica. Here, we investigated in detail and correlated the adsorption kinetics of annexin A5 on SLBs, supported on silica and on mica, with the protein's 2D self-assembly behavior. For this study, quartz crystal microbalance with dissipation monitoring and ellipsometry were combined with atomic force microscopy. We find, in agreement with previous studies, that the adsorption behavior is strongly dependent on the concentration of dioleoylphosphatidylserine (DOPS) in the SLB and the calcium concentration in solution. The adsorption kinetics of annexin A5 are similar on silica-SLBs and on mica-SLBs, when taking into account the difference in accessible DOPS between silica-SLBs and mica-SLBs. In contrast, 2D crystals of annexin A5 form readily on mica-SLBs, even at low protein coverage ($\leq$10%), whereas they are not found on silica-SLBs, except in a narrow range close to maximal coverage. These results enable us to construct the phase diagram for the membrane binding and the states of 2D organization of annexin A5. The protein binds to the membrane in two different fractions, one reversible and the other irreversible, at a given calcium concentration. The adsorption is determined by the interaction of protein monomers with the membrane. We propose that the local membrane environment, as defined by the presence of DOPS, DOPC, and calcium ions, controls the adsorption and reversibility of protein binding.

INTRODUCTION

The formation of protein crystals, both in three dimensions and in two dimensions, occupies an instrumental place in structural biology, enabling molecular structure resolution, down to the atomic level, by x-ray crystallography (1) and transmission electron microscopy (TEM) (2). Procedures to obtain crystals have remained largely empirical, though recent years have witnessed a tendency toward rationalization of macromolecular crystallization (3–7).

Two-dimensional (2D) crystals have been implicated as intermediates in the formation of three-dimensional (3D) crystals (8) and 2D nucleation has been identified as one of the mechanisms by which 3D crystals grow (9). Two-dimensional crystallization at interfaces is highly complex (3), involving a multitude of processes, such as the transport of proteins to the interface, their adsorption and diffusion in two dimensions, nucleation, and growth of the crystal. Two-dimensional self-assembly thus presents a challenging problem in fundamental science, which becomes particularly interesting as the limitation to two dimensions is expected to induce a distinctly different behavior as compared to 3D systems (10).

Biological membranes and membrane models constitute a natural 2D space for diffusion and 2D ordering of membrane proteins (e.g., bacteriorhodopsin (11), aquaporin (12)) and membrane-associated proteins (e.g., streptavidin (6,13)).

Annexin A5 is the prototype of a family of proteins that share the property of binding to negatively charged phospholipids, in particular dioleoylphosphatidylserine (DOPS), in a calcium-dependent manner (14). Annexin A5 is commonly observed to undergo 2D crystallization on lipid monolayers at the air-water interface (15–18) and on mica-supported lipid bilayers (SLBs) containing DOPS (5,19). The protein's self-assembly properties have been suggested to be relevant for its biological function (20).

Using ellipsometry (21,22), quartz crystal microbalance with dissipation monitoring (QCM-D) (23), fluorescence spectroscopy (24–26), and biochemical techniques (27,28), the adsorption of the protein to various types of lipid membranes has been characterized in detail. Using TEM on lipid monolayers and atomic force microscopy (AFM) on SLBs, a trimeric intermediate (29) and two common crystal forms—a low-density form with p6 symmetry (16,18,19) and a high-density form with p3 symmetry (29,30)—have been identified. The phase transitions between these states have been investigated (5,17,31), resulting in the self-assembly scheme presented in Fig. 1 (23). In some cases, other crystalline assemblies have also been observed (18).

Although the intermediates of the self-assembly process and the adsorbed amounts of annexin A5 have been characterized extensively, relatively little is known about the kinetics of adsorption and self-assembly, a fundamental parameter for the description of the 2D crystallization process. Here we characterize, in detail, the binding (adsorption and desorption) and the 2D self-assembly of annexin A5 on lipid bilayers. Two parameters of importance for binding, the

Submitted April 13, 2005, and accepted for publication June 29, 2005.

Address reprint requests to Alain R. Brisson, E-mail: a.brisson@iecb.u-bordeaux.fr.

Ralf P. Richter's present address is Dept. of Biophysical Chemistry, Institute of Physical Chemistry, Heidelberg University, Im Neuenheimer Feld 253, 69 120 Heidelberg, Germany.

0006-3495/05/11/3372/14 $2.00

doi: 10.1529/biophysj.105.064337

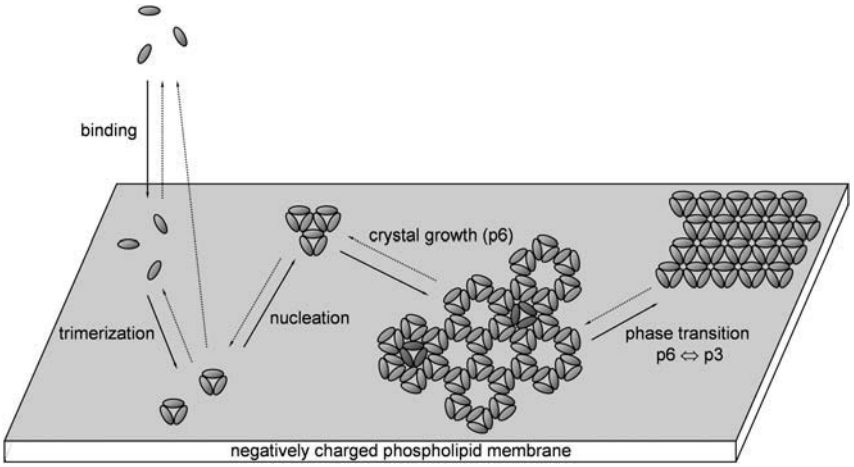

FIGURE 1 Schematic description of the 2D self-assembly of annexin A5 on a negatively charged phospholipid membrane in the presence of calcium ions, according to Govorukhina et al. (23). Monomeric annexin A5 binds to the membrane in a calcium-dependent manner where it forms trimers. The trimers crystallize in two dimensions. The holes in the honeycomb-like lattice of p6 symmetry can be filled by additional noncrystalline trimers (marked in *dark gray*), also called ''central trimers''. At high protein coverage, a phase transition of first order into a more densely packed crystal form with p3 symmetry can occur.

calcium concentration in solution and the DOPS content in the bilayer, were systematically varied over a wide range.

In a previous study (32) we observed, unexpectedly, that annexin A5 does not form 2D crystals on SLBs supported on silica: trimers were found on silica under conditions where 2D crystals with p6 symmetry were observed on mica, even though the SLBs' main characteristics are expected to be similar on both surfaces. To explain this intriguing result we investigate the membrane binding and self-assembly of annexin A5 both on mica-SLBs and on silica-SLBs.

Our experimental approach consists in combining AFM and QCM-D, complemented by ellipsometry. We have recently demonstrated the strength of combining AFM and QCM-D for the characterization of processes that involve the adsorption and 2D self-organization of biomolecules at the solid-liquid interface (33–35). AFM gives access to structural information, spatially resolved on the nanometer scale, whereas QCM-D and ellipsometry allow following quantitatively the overall binding dynamics, which renders the techniques highly complementary. Here, the combined study allows correlating the protein's 2D crystallization with its binding behavior.

MATERIALS AND METHODS

Materials

Dioleoylphosphatidylcholine (DOPC), dipalmitoylphosphatidylcholine (DPPC), and dioleoylphosphatidylserine (DOPS) were purchased from Avanti Polar Lipids (Alabaster, AL). Other chemicals were purchased from Sigma (St. Louis, MO). Ultrapure water with a resistivity of 18.2 MΩ was used (Maxima, USF ELGA, Trappes, France).

Muscovite mica disks of 12 mm diameter were purchased from Metafix (Montdidier, France). Plates of silicon wafer of (11 × 11) mm^2 (for AFM) were provided by the CEA (Grenoble, France). Slides of (40 × 8) mm^2 (for ellipsometry) were cut from silicon wafers from Wacker Chemitronic (n-type, phosphorus doped), purchased from Aurel GmbH (Landsberg, Germany). QCM-D sensor crystals (5 MHz), reactively sputter coated with 50 nm silicon oxide, were purchased from Q-SENSE (Gothenburg, Sweden). Low viscosity epoxy glue (EPOTEK 377) for mica gluing was purchased from Gentec Benelux (Waterloo, Belgium).

A buffer solution made of 150 mM NaCl, 3 mM NaN_3, and 10 mM HEPES, pH 7.4, was prepared in ultrapure water, and EDTA or $CaCl_2$ were added as indicated. Small unilamellar vesicles (SUVs) of desired lipid mixture were prepared by sonication as described earlier (33). For SLB formation, vesicle suspensions were diluted to 0.1 mg/mL in buffer containing 2 mM $CaCl_2$.

Expression and purification of recombinant rat annexin A5

The rat annexin A5 coding sequence was excised by *Nco*I digestion from a pKK233-2-annexin-A5 expression vector (36) and subcloned into the expression vector pGEF between two *Nco*I restriction sites, resulting in the pGEF-A5 expression vector. *Escherichia coli* BL21 (DE3) cells were transformed by heat shock with plasmid pGEF-A5. Cells were plated out on LB medium containing ampicillin (100 μg/mL), and incubated overnight at 37°C. A single colony was collected and grown at 37°C. Protein expression was induced by 0.4 mM IPTG for 16 h at 30°C. The cells were harvested by centrifugation (10 min, 6700 × *g*) and the pellet was resuspended in an appropriate volume of buffer containing 10 mM Tris, 1 mM EDTA, 0.01% NaN_3, 10% glycerol, pH 7.5. The cell suspension was sonicated at 4°C with a Branson sonicator operated in a pulse mode consisting of five steps of sonication at 13 W for 1 min with 15-s intervals. Membrane fragments and large debris were separated by centrifugation at 48,000 × *g* for 1 h at 4°C. The supernatant, referred to as cell soluble extract, was collected and stored until use at 4°C.

The cell soluble extract was filtered over 0.22-μm filters and applied in 5-mL fractions to a Superdex 75 exclusion column (Amersham BioSciences, Uppsala, Sweden) preequilibrated with a buffer containing 20 mM Tris, pH 8, 0.02% NaN_3 (buffer A). Elution of proteins was performed with buffer A. The fractions were analyzed by SDS-PAGE. The fractions containing annexin A5 were pooled and purified by anion-exchange chromatography with a MonoQ HR5/5 column (Amersham BioSciences) preequilibrated with buffer A. Elution was performed with a 0–0.5 M NaCl gradient in buffer A. The fractions were analyzed by SDS-PAGE.

Quartz crystal microbalance with dissipation monitoring

Quartz crystal microbalance with dissipation monitoring (QCM-D) measurements (37) were performed with the Q-SENSE D300 system equipped with an axial flow chamber (QAFC 302) (Q-SENSE AB, Gothenburg, Sweden). Briefly, upon interaction of (soft) matter with the surface of a sensor crystal, changes in the resonance frequency, *f*, related to attached mass (including coupled water), and in the dissipation, *D*, related to frictional (viscous) losses in the adlayer, are measured with a time resolution of better than 1 s.

Silica-coated QCM-D sensors were cleaned by two cycles of exposure to 2% sodium dodecyl sulfate solution for 15 min, rinsing with ultrapure water, blow-drying with nitrogen, and exposure to ultraviolet light (UV)/ozone (33) (BHK, Claremont, CA) for 10 min. Cleaned substrates were stored in air and again exposed to UV/ozone (10 min) before use. Mica-coated QCM-D sensors were prepared and verified to operate stably according to a previously described protocol (34). Briefly, mica sheets were glued to the QCM-D sensors using epoxy glue. The glued mica sheets were cleaved until sufficiently thin mica layers and stably operating sensors were obtained.

Measurements were performed in exchange mode (described in detail elsewhere (33)), if not otherwise stated. The exchange mode allows following processes of adsorption and surface adlayer changes in situ while sequentially exposing different solutions to the supports. In this mode the fluid in the measurement chamber is generally still. Occasionally, flow mode was employed, i.e., the solution was continuously delivered to the measurement chamber (flow speed 80 μL/min) by the aid of a peristaltic pump (ISM832A, Ismatec, Zürich, Switzerland) (38). The working temperature was 24°C.

Resonance frequency and dissipation were measured at several harmonics (15, 25, 35 MHz) simultaneously. If not stated otherwise, changes in dissipation and in normalized frequency ($\Delta f_{norm} = \Delta f_n/n$, with n being the overtone number) of the fifth overtone ($n = 5$, i.e., 25 MHz) are presented. Adsorbed masses, Δm, are calculated according to the Sauerbrey equation (39), $\Delta m = -C \cdot \Delta f_{norm}$, with the mass sensitivity constant $C = 17.7$ ng/cm^2/Hz for 5 MHz sensor crystals. The changes in the viscosity and density of the buffer upon variation of its content in $CaCl_2$ or EDTA significantly influenced the QCM-D signal. These changes were accounted for by calibration against a clean silica-coated QCM-D sensor.

For the transfer of QCM-D sensors with adsorbed material from the QCM-D chamber to the AFM, sensors were unmounted with the aid of a suction holder (Meni CUP, Menicon Pharma, Illkirch Graffenstaden, France), ensuring that the sample remained permanently covered with liquid.

Ellipsometry

Ellipsometry is an optical technique based on the measurement of changes in the ellipsometric angles, Δ and Ψ (40,41), of elliptically polarized light upon reflection off a planar surface. These changes are sensitive to the presence of thin deposited films and, consequently, the method allows monitoring adsorption phenomena in situ. The employed null-ellipsometer setup with a time resolution of 10–15 s has been described in detail (40,42). In the frame of this study we consider the change in the angle Δ only, which is approximately proportional to the (dry) protein mass adsorbed to mica or silica (43).

Before first use, silicon slides were precleaned by exposure to concentrated detergent solution (Sparkleen, Calgon, Pittsburg, PA), rinsing with water, exposure to 30% chromic sulfuric acid (80°C for 20 min) and extensive rinsing in ultrapure water. Further cleaning before each use was performed as described for silica-coated QCM-D sensors. Mica disks were rendered opaque on their back side with emery paper and glued on an aluminum slide over a hole (8 mm diameter) using melted wax (44). Uniform mica surfaces were obtained by cleavage of the front side with adhesive tape and used immediately.

Measurements were performed in an open cuvette system (42), at room temperature. The buffer solution (~3 mL) was stirred with a magnetic stirrer (~1000 rpm). Samples were pipetted at appropriate concentrations into the solution. Such a setup generates constant adsorption rates provided the adsorption is mass-transport limited (45). Rinses were realized by injecting ~30 mL of buffer (injection rate ~1 mL/s) while simultaneously withdrawing excess liquid.

Atomic force microscopy

Atomic force microscopy (AFM) measurements were performed in liquid using a Nanoscope IV-Multimode (VEECO, Dourdan, France), equipped with a J-scanner (120 μm). Before use, the contact mode fluid cell was washed in successive baths of ethanol and ultrapure water, followed by extensive rinsing in ethanol and blow-drying in a stream of nitrogen. Tubings and O-ring were sonicated in ethanol and water, rinsed with ethanol, and blow-dried in nitrogen. Oxide-sharpened silicon nitride cantilevers with a nominal spring constant of 0.06 N/m (Digital Instruments, Santa Barbara, CA) were exposed to UV/ozone (BHK, Claremont, CA) for 10 min before use.

Silicon plates were cleaned as described for the silica-coated QCM-D sensors, attached to Teflon-coated (BYTAC, Norton, OH) metal disks using double-sided tape (TESA, Hamburg, Germany), and immediately covered with buffer solution. Mica disks were glued to Teflon-coated metal disks using the epoxy glue, cleaved with adhesive tape, and immediately covered with buffer solution. For AFM investigations subsequent to QCM-D measurements, mica-coated QCM-D sensors, covered with the sample, were attached to Teflon-coated metal disks using double-sided tape and installed on the AFM scanner.

Contact mode images were acquired at scanning rates of 4–8 Hz while manually adjusting the force to a minimum (<200 pN). Images were second-order plane fitted and subsequently zero-order flattened except otherwise stated.

RESULTS

Adsorption of annexin A5 on silica-SLBs

We employed the QCM-D technique to characterize the adsorption of annexin A5 on silica-SLBs. The measurement shown in Fig. 2, obtained for an SLB formed from SUVs of DOPC/DOPS (molar ratio 9:1), is representative of our experimental approach.

The QCM-D response upon exposure of SUVs to the support (Fig. 2, at 0 min) reveals, as expected, a characteristic two-phase behavior, reflecting the initial adsorption of intact vesicles, which is followed by the formation of an SLB (33,46). The final frequency shift of -25 ± 1 Hz and the low dissipation shift of $<0.2 \times 10^{-6}$ confirm the formation of a lipid bilayer that entirely covers the support with no or only minor defects (35,47).

Incubation of the SLB with annexin A5 (Fig. 2, *solid arrows*) leads to adsorption of the protein, witnessed by the decreases in frequency, in a calcium-dependent manner. As expected (21,26), increasing calcium concentrations enhanced protein binding: while a negligible amount of annexin A5 bound at 200 μM $CaCl_2$ (Fig. 2, at 10 min), a coverage of $\Delta f = -18 \pm 0.5$ Hz was reached for 200 mM (Fig. 2, at 89 min). As demonstrated in Fig. 2 and observed for all measurements, the dissipation remained almost unchanged throughout the entire process of protein adsorption, suggesting that the protein associates tightly with the SLB.

The adsorption of annexin A5 at 20 mM $CaCl_2$ (Fig. 2, at 54 min) reveals some typical properties of the immobilization of annexin A5 on silica-SLBs. The adsorption of annexin A5 reached equilibrium within a few minutes after exposure for the employed protein concentrations. The final adsorbed amounts changed little upon increase of the annexin A5 concentration from 20 to 80 μg/mL. Only a part of annexin A5 (here corresponding to 3 Hz) was displaced upon rinsing in a buffer solution that contained the same amount of

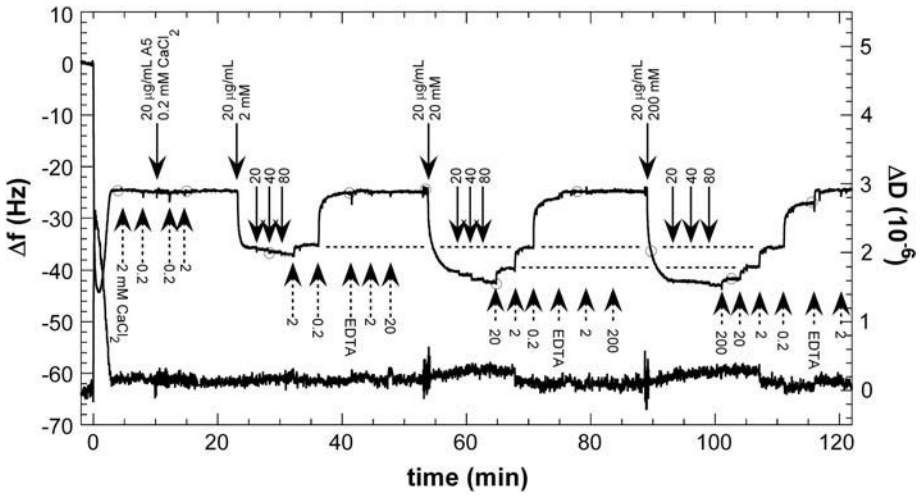

FIGURE 2 QCM-D response (frequency, Δf (-○-), and dissipation, ΔD (*long dash*), at 35 MHz) for a typical measurement to investigate the adsorption of annexin A5 to SLBs. The SLB was formed by incubation of SUVs of DOPC/DOPS (molar ratio 9:1) on silica (0 min). The adsorption of annexin A5 at various concentrations (injections indicated by *solid arrows*, at concentrations given in μg/mL) was measured in the presence of 0.2, 2, 20, and 200 mM $CaCl_2$ (as indicated). Dotted arrows indicate rinses accompanied with changes in the calcium concentration (in millimolar or EDTA, as indicated). The horizontal dotted lines indicate the levels of bound annexin A5 after rinses in 20 mM (*lower line*) and 2 mM (*upper line*) $CaCl_2$, which are independent of the incubation history. Rinses in EDTA lead to complete unbinding of annexin A5.

calcium as used during adsorption. Additional rinses (Fig. 2) or continuous flow (in flow mode, data not shown) with such a buffer did not lead to further release of annexin A5. This provides indications for the presence of two different populations of bound annexin A5; for a given calcium content, a part of annexin A5 can easily be displaced (reversible binding) whereas the rest binds irreversibly. The term ''irreversible binding'' refers to annexin A5 binding in a protein-free solution containing a given calcium concentration. Note that the adsorbed amount corresponding to the fraction of irreversibly bound annexin A5 could also be reached by incubation with lower protein concentrations (1 μg/mL or below, in flow mode, not shown). Protein concentrations in the range of 20–80 μg/mL affected only the amount of reversibly bound annexin A5.

Annexin A5 could, however, be displaced by rinsing with decreasing calcium concentrations or in the presence of the calcium chelator EDTA (Fig. 2, *dotted arrows*). For DOPC/DOPS (9:1), Δf returned to the value characteristic for a bare SLB at 20 μM $CaCl_2$ or in the presence of EDTA. We further tested the reproducibility of the experimental approach by performing several cycles of incubation with annexin A5 at 20 mM $CaCl_2$, followed by rinses in EDTA-containing buffer, on the same SLB (not shown). We obtained identical QCM-D responses, which confirms that the silica-SLB can be recovered without significant perturbations (21) and justifies our approach to perform several incubations with annexin A5 on the same bilayer.

We note also that the amount of irreversible binding is the same independently of the way the protein was incubated (c.f. Fig. 2, *horizontal dotted lines* for 2 and 20 mM $CaCl_2$). The same phenomenon was observed for all measurements conducted on silica-SLBs, indicating that the reversibility of protein binding is independent of the history of annexin A5 deposition over the investigated timescale. In consequence, our results indicate that the amount of irreversibly bound annexin A5 is entirely determined by the calcium concentration in solution, [Ca], and the DOPS content, [DOPS], in the SLB.

Based on these observations, we investigated the equilibrium adsorbed amounts, Δf_e, of annexin A5 on silica-SLBs in a systematic manner as a function of [DOPS], [Ca], and the bulk concentrations of the protein, [A5]. The results are summarized in Fig. 3 and Table 1.

As already reported by others (14,21,26,28), we found that the adsorption of annexin A5 increases with [Ca] and [DOPS]. The dependence is sigmoidal for both [DOPS] (at a given [Ca], Fig. 3) and [Ca] (at a given [DOPS], not shown). In particular, the calcium concentrations required to reach the half-maximal frequency shift for 0, 5, and 20%

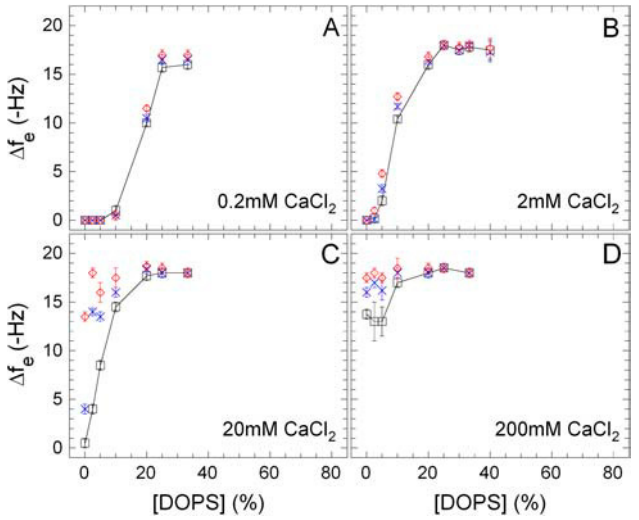

FIGURE 3 Equilibrium adsorbed amounts, given by the shifts, Δf_e, in QCM-D frequency, of annexin A5 on silica-SLBs, as a function of the SLB's DOPS content, [DOPS], and the concentration of annexin A5 for 0.2 (*A*), 2 (*B*), 20 (*C*), and 200 mM (*D*) $CaCl_2$. Bulk concentrations of annexin A5 were 20 (×, *blue*) and 80 μg/mL (◇, *red*), respectively. The amounts of annexin A5 remaining after rinsing in buffer are also indicated (□, *black*) and connected by lines to guide the eye.

TABLE 1 Conditions of [DOPS] and [Ca] required for half-maximal binding of annexin A5

	[Ca] (mM)	[DOPS] (%)
Fig. 3*	0.2	19 ± 1
	2	9.5 ± 0.5
	20	5.0 ± 0.5
	20..200	0
Fig. 6†	0.2	17 ± 2
	2	10 ± 1
	20	6 ± 1
	20..200	0
Andree et al.‡	0.036 ± 0.013	100
	0.22 ± 0.06	20
	1.5 ± 0.5	5
	8.6 ± 2.5	1
	>30	0
Pigault et al.§	0.057	50
	0.13	25
	1	17
	3	9.1
	7	3.8
	12	2
	68	1
Govorukhina et al.¶	50	0

*Experimental results obtained by QCM-D on silica-SLBs for the amount of irreversibly bound annexin A5.

†Experimental results obtained by QCM-D on mica-SLBs for the amount of irreversibly bound annexin A5; the accessible DOPS content is stated as determined by Richter et al. (38) (see Fig. 6 for details).

‡From Andree et al. (21), obtained with SLBs formed by Langmuir-Blodgett deposition.

§From Pigault et al. (26), obtained with large unilamellar vesicles.

¶From Govorukhina et al. (23), obtained by QCM-D on silica-SLBs at [A5] = 10 μg/mL.

DOPS are close to those reported by Andree et al. (21) on silica-SLBs formed by Langmuir-Blodgett deposition (c.f. Table 1 and Fig. 7 *A*). We note that annexin A5 binds also to pure DOPC at high calcium concentrations (≥20 mM), as discussed in previous work (23). No adsorption of annexin A5 was observed at ≤20 mM $CaCl_2$.

The maximum adsorbed amount of annexin A5 was $\Delta f_{max} = -18 \pm 0.5$ Hz, over the entire range of [DOPS] investigated, suggesting that this value corresponds to the full coverage of the SLB with a monolayer of annexin A5. This frequency shift corresponds to a total mass (including coupled water) of 319 ± 9 ng/cm^2 (34).

Three different regimes can be discerned in terms of reversibility of binding upon rinsing with protein-free solution containing the same amount of [Ca] as used for adsorption (Fig. 3):

1. Once the plateau of maximal coverage is reached (i.e., for elevated [DOPS]), annexin A5 binding was fully irreversible.
2. In the range of intermediate binding (i.e., around the inflection point of the sigmoidal curve), most of the protein was irreversibly bound for [Ca] ≤ 2 mM. The reversibly bound fraction corresponded at most to 3 Hz for the employed annexin A5 concentrations.
3. In contrast, binding to pure DOPC, which is considerable at 20 mM calcium and more, was completely (for 20 mM) or partially (for 200 mM) reversible. Also for SLBs containing small amounts of DOPS (up to 5%) a substantial part of the adsorbed amount is reversible at [Ca] ≥ 20 mM.

Adsorption kinetics of annexin A5

The adsorption of annexin A5 at 200 mM $CaCl_2$ and 20 μg/mL protein concentration (c.f. Fig. 2, 89 min) is representative for the adsorption kinetics that we observed under all employed conditions that led to (close to) maximal coverage. We note that it takes <5 min for the adsorption to reach completion, which is in the time range expected for mass-transport limited adsorption. With the employed setup of still liquid, the adsorbed amount is given by $\Gamma = 2c\sqrt{Dt/\pi}$ for mass-transport limited adsorption (45). Assuming a bulk diffusion coefficient, $D = 60\ \mu m^2/s$, and a concentration, $c =$ 20 μg/mL, of the protein, this corresponds to a time, $t \approx$ 200 s, to reach a coverage of $\Gamma = 250$ ng/cm^2 (dry mass). To further investigate the adsorption kinetics, we performed measurements by ellipsometry under experimental conditions that provide constant adsorption rates under mass-transport limited conditions (45). As demonstrated in Fig. 4, the adsorption curve is linear up to >65% of the final coverage, confirming that the adsorption is indeed to a large extent mass-transport limited (21). Even though some deviations from the mass-transport limited regime occur at higher coverage, the adsorption goes quickly to completion.

2D self-assembly of annexin A5 on silica-SLBs

We have previously reported by AFM, that 2D crystals of annexin A5 are not present on silica-SLBs formed with DOPC/DOPS (4:1) at 2 mM $CaCl_2$ (32), whereas 2D crystals are commonly observed on mica (5). Here we have extended our AFM investigations to a larger range of DOPS concen-

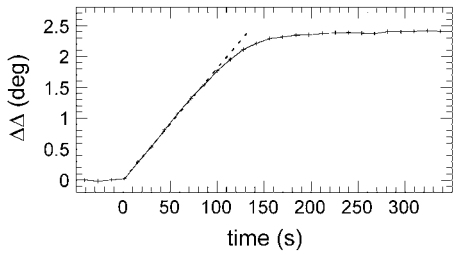

FIGURE 4 Adsorption of 2 μg/mL annexin A5 on a silica-SLB made of DOPC/DOPS (4:1) as measured by ellipsometry in stirred buffer at 2 mM $CaCl_2$. The adsorption rate is constant (*dotted line*), indicating mass-transport limited adsorption, until >65% of the final coverage.

trations (0–30%). Two different responses could be observed as a function of protein coverage.

Under conditions for which maximal protein coverage was expected according to our QCM-D results, a mosaic of ordered domains could be discerned that covered the entire surface (Fig. 5 *A*). Individual domains had a size of typically <50 nm. The limited domain size and resolution currently prohibit an unambiguous determination of the crystal form. Nevertheless the available structural information is compatible with the p3 crystal form (Fig. 5 *A*, *bottom inset*), whereas we can exclude the presence of the p6 crystal form that is easily distinguishable (*top inset*) (30).

Under conditions for which substantial but submaximal protein coverage was expected (corresponding to frequency shifts from −10 to −17 Hz), we did not find any supramolecular structures exhibiting long-range order, despite numerous trials and the fact that the support was flat enough to obtain 2D protein crystals in the case of streptavidin (32). Neither did we find the micrometer-sized domains, that are characteristic of the 2D crystals of p6 symmetry and easily visible on incompletely covered mica-SLBs (c.f. Fig. 10) (19).

Instead, we observed characteristic jumps of the AFM tip on an otherwise fairly smooth surface that occurred as a function of the scanning speed and force and led to images exhibiting two different apparent height levels, separated by ~2 nm (Fig. 5 *B*). These jumps were not observed on SLBs that had not been incubated with annexin A5, confirming that they are due to the presence of the protein. We suggest that the ''water-skiing effect,'' earlier reported by Rädler et al. (48) on lipid bilayers, provides a reasonable explanation for our observation: at low forces and/or high scanning speed the tip slides over the layer of annexin A5 molecules whereas it jumps down through the layer at slightly increased forces and/or decreased scanning speed. Indeed, the observed jump height of ~2 nm (Fig. 5 *B*, *inset*) is only slightly lower than the height (2.6 nm) of 2D crystals of annexin A5 (19). The occurrence of such sliding and indentation implies that annexin A5 is laterally mobile. We have reported earlier (32) that scratches can be introduced in the annexin A5 layer and that these scratches heal quickly, providing further evidence for the presence and for the lateral mobility of annexin A5 on silica-SLBs.

Taken together, our data indicate that the low density crystal form with p6 symmetry is not present on silica-SLBs. This result contrasts remarkably with those previously reported on mica (5,19).

We note that the silica supports employed for the QCM-D measurements were considerably rougher than the supports used for the AFM investigations (32). As roughness is not expected to improve the propensity to crystallization, we consider it unlikely that annexin A5 does crystallize on any of the silica supports employed in this study before close to maximal surface coverage is reached.

The presence of annexin A5 trimers

Evidence has accumulated in previous studies, that the surface-induced oligomerization into trimers precedes the 2D crystallization of annexin A5 (18,23). Provided our observations that 2D crystals do not form on silica-SLBs, an obvious question is whether trimers do actually form on silica-SLBs. The high lateral mobility of the protein renders the imaging of monomers or oligomers of annexin A5 by AFM difficult and we could not find direct evidence for the presence of annexin A5 trimers on SLBs composed of DOPC and DOPS only. The lateral diffusion of SLB-bound annexin A5 can be as high as the diffusion of the lipid molecules to which it is bound (49), i.e., in the order of 1 $\mu m^2/s$. This is more than the area covered by the AFM tip (0.01 $\mu m^2/s$) under common

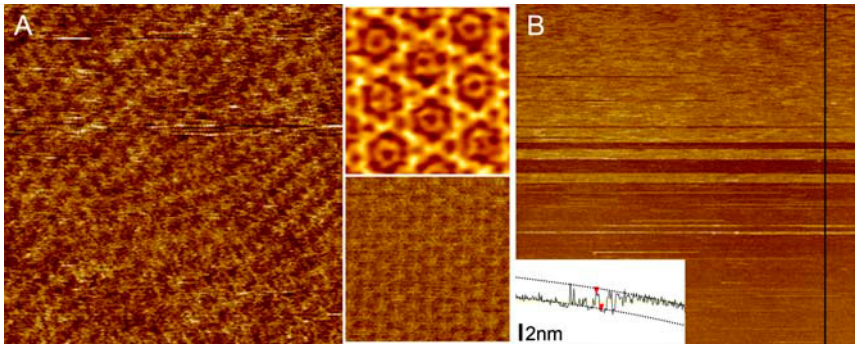

FIGURE 5 (*A*) Two-dimensional ordered organization of annexin A5 on silica-SLBs (DOPC/DOPS (2:1)) in 2 mM $CaCl_2$. Ordered domains of 50 nm and less in size can be discerned, which cover the surface completely. The ordered structure is compatible with the p3 crystal form (*bottom inset*, obtained on a mica-SLB made of DOPC/DOPS (1:4) in 0.2 mM $CaCl_2$), but not with the p6 crystal form (*top inset*, adapted from Reviakine et al. (19)). Image size (z-limit): 150 nm (2.5 nm). (*B*) Tracking the presence of annexin A5 on silica-SLBs by AFM. While imaging from top to bottom, the applied force increased, due to thermal drift, from ~50 to ~200 pN. These slight variations led to jumps of 2 nm in the height (*cross section* in *inset*). This effect is attributed to the ''water-ski'' effect: at lowest forces (*top*) the tip is sliding over the disordered layer of laterally mobile annexin A5, whereas it jumps down to the underlying SLB at slightly higher forces (*bottom*). Dotted lines (*inset*) mark the two height levels that correspond to the top of the annexin A5 (*top dotted line*) layer and the top of the SLB (*bottom dotted line*), respectively. Annexin A5 was incubated on SLBs of DOPC/DOPS (9:1) in 2 mM $CaCl_2$. The image was first-order plane-fitted. Image size (z-limit): 2.5 μm (10 nm).

high-resolution imaging conditions. The comparison illustrates the difficulties associated with imaging mobile proteins on SLBs. It should, however, be noted that AFM images of mixtures of DOPC, DOPS, and DPPC showed that trimers of annexin A5 can exist on silica-SLBs (32). The fact that trimers of annexin A5 could in this case be resolved by AFM may be explained by a decreased lateral diffusion of the lipids due to the presence of DPPC lipids in the SLB.

Adsorption of annexin A5 on mica-SLBs

Having investigated the adsorption and 2D self-assembly of annexin A5 on silica-SLBs we now turn to its deposition on mica-SLBs. Fig. 6 gives an overview of the (equilibrium) adsorbed amounts.

When comparing the adsorption behavior at nominal [DOPS] (Figs. 6, *A–D*, and 3), i.e., the DOPS content given by the molar mixing ratio of DOPC and DOPS in the SUVs, we observe that the adsorbed amounts on mica are generally lower than on silica for a given [DOPS]. This result is not unexpected. As shown earlier (38), the interleaflet distribution of DOPS in mica-SLBs is asymmetrical, leading to DOPS concentrations in the bulk-facing leaflet, i.e., accessible [DOPS], which are considerably lower than for silica-SLBs.

If we take into account the difference in accessible [DOPS] between SLBs on silica and on mica, according to earlier quantifications (38) (Fig. 6, *E–H*), we find that the adsorption behavior of annexin A5 on both surfaces is, in many aspects, similar. The overall influence of [Ca] and [DOPS] on the annexin A5 adsorption is the same, within experimental error, as witnessed by identical values for [Ca] and [DOPS] to reach the half-maximum frequency shifts (Table 1). As for silica, binding is entirely irreversible at high [DOPS] and [Ca]. Also, the adsorption of annexin A5 on pure DOPC is very similar on both surfaces, exhibiting a high degree of reversibility. On the other hand, mica-SLBs show slightly higher amounts of reversible binding at an intermediate range of [DOPS] and for [Ca] $\leq$ 2mM.

2D crystallization of annexin A5 on mica-SLBs

In strong contrast to silica-SLBs, annexin A5 2D crystals could be observed on all types of mica-SLBs investigated. Fig. 7 *A* provides an overview of the self-assembly structures found by AFM, and the adsorption behavior found by QCM-D, as a function of [DOPS] and [Ca]. Three different regimes can be discerned: i), no adsorption takes place; crystalline patches with ii), p6 symmetry and iii), p3 symmetry are present. In all investigated cases and in agreement with previous studies (5), exclusively the p6 crystal form could be observed at low coverage of annexin A5 and the p3 crystal form started to appear only after an intermediate of complete surface coverage with p6 crystals was reached. The combination of QCM-D and AFM on mica allowed us to identify frequency shifts of $\Delta f_{p6} = -17.8 \pm 1$ Hz and $\Delta f_{p3} = -19 \pm 1$ Hz as representative for the presence of complete crystalline layers of p6 and p3 symmetry, respectively (34).

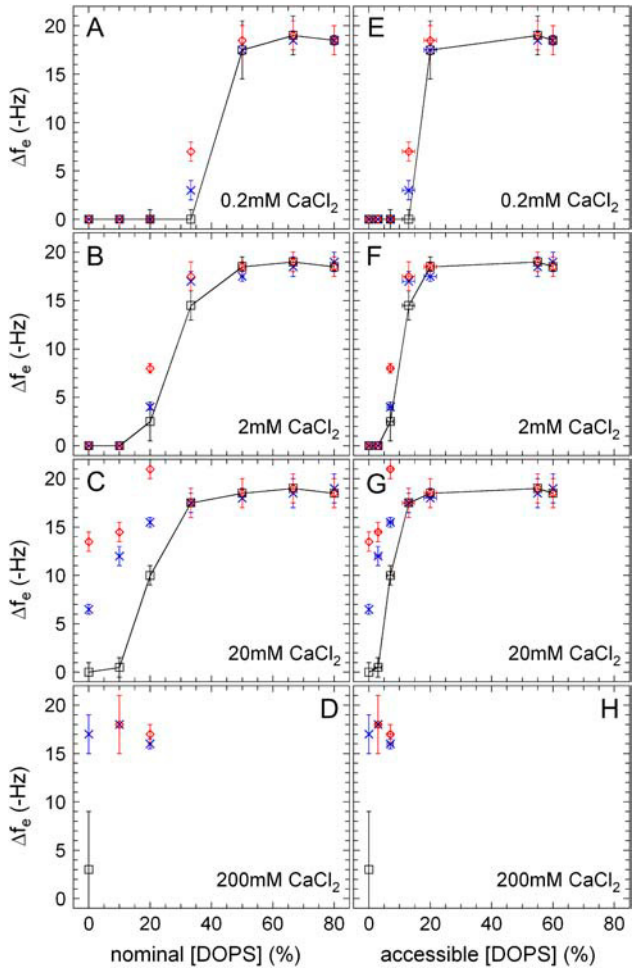

FIGURE 6 Adsorbed amounts, given in QCM-D frequency shifts, Δf_e, of annexin A5 on mica-SLBs, as a function of the SLB's DOPS content, and the concentration of annexin A5 for 0.2 (*A*, *E*), 2 (*B*, *F*), 20 (*C*, *G*), and 200 mM (*D*, *H*) $CaCl_2$. Annexin A5 was incubated at 20 ($\times$, *blue*) and 80 μg/mL ($\diamond$, *red*), respectively. The amounts of annexin A5, remaining after rinsing in buffer are also indicated ($\square$, *black*) and connected by lines to guide the eye. The abscissa shows the nominal DOPS content (*A–D*), given by the molar mixing ratio of DOPC and DOPS, and the accessible DOPS content (*E–H*), i.e., the DOPS content in the bulk-facing leaflet of the SLB. The accessible DOPS contents were determined elsewhere (38), taking silica-SLBs as reference, to be 3 ± 1, 7 ± 1, 13 ± 2, 20 ± 2, >55, and >60% for nominal DOPS contents of 10, 20, 33, 50, 67, and 80%, respectively.

It is remarkable, that complete p6 crystals could also be found on pure DOPC at [Ca] $\geq$ 20 mM (Fig. 7 *B*) (23). In agreement with QCM-D results, the annexin A5 crystal was found to disappear upon rinsing in 20 mM $CaCl_2$.

Kinetics of adsorption and of 2D self-assembly of annexin A5 on mica-SLBs

With the aim to characterize the relationship between adsorption and 2D self-assembly, we investigated the kinetics of both processes in more detail.

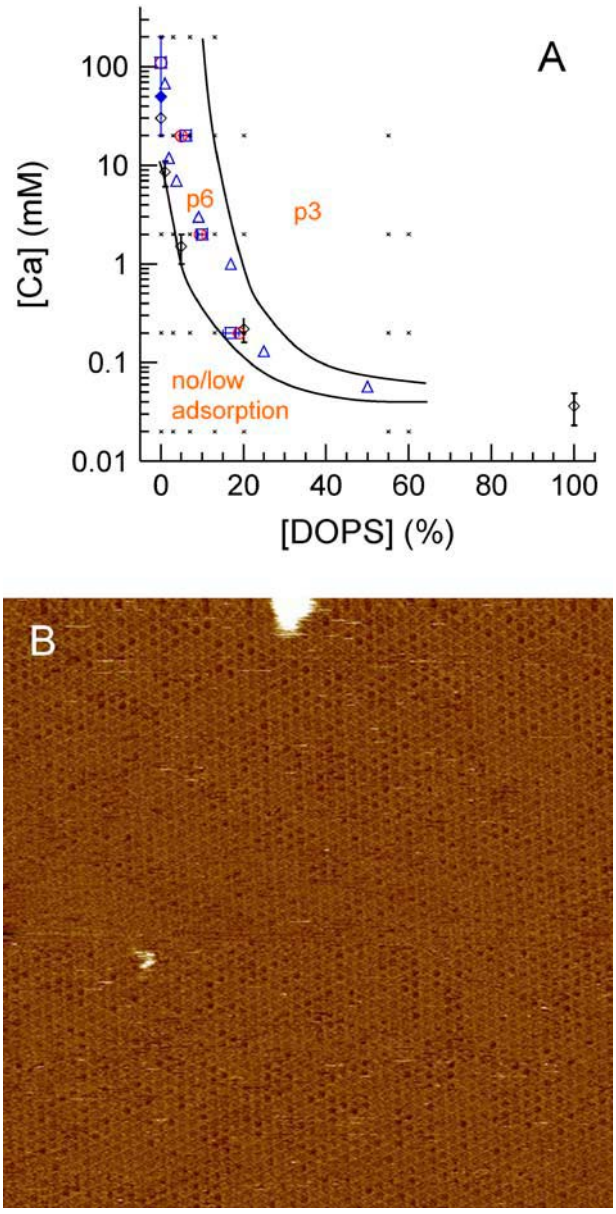

FIGURE 7 (*A*) Diagram of the state of adsorption and 2D organization of annexin A5 on mica-SLBs as a function of accessible [DOPS] and [Ca]. A pair of conditions of ([DOPS],[Ca]) is counted as belonging to the zones p6 and p3, if at least partial coverage with respective crystalline lattice has been observed under these conditions. Conditions where approximately half-maximal binding was reached, according to Fig. 3 (○, *red*), Fig. 6 (□, *blue*), Andree et al. (21) (◇, *black*), Pigault et al. (26) (Δ, *blue*), and Govorukhina et al. (23) (♦, *blue*), are indicated. Experimentally investigated data points are indicated (×). (*B*) Annexin A5 crystallizes even on pure DOPC. The p6 crystal was obtained by AFM after incubation of 20 μg/mL annexin A5 (~20 min) at 200 mM $CaCl_2$, and observed to cover the entire surface. Image size (z-limit): 1 μm (5 nm).

Adsorption kinetics until formation of a complete layer of p6 crystals

A representative example of ellipsometric measurements on mica is shown in Fig. 8. The adsorption of annexin A5 on

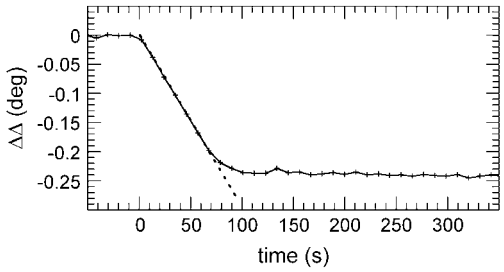

FIGURE 8 Adsorption of 5 μg/mL annexin A5 on a mica-SLB made of DOPC/DOPS (1:2) as measured by ellipsometry in stirred buffer at 0.2 mM $CaCl_2$. The adsorption rate is constant (*dotted line*), indicating mass-transport limited adsorption, until >70% of the final coverage. Adsorption results in negative shifts in Δ on mica, in contrast to positive shifts on silica (Fig. 4).

SLBs made of DOPC/DOPS (1:2) in 0.2 mM $CaCl_2$ showed a linear adsorption regime, indicating mass-transport limited adsorption, until >70% of the apparent equilibrium coverage of $\Delta\Delta = -0.24°$, which was reached quickly (after ~2 min). Based on further ellipsometry data (not shown) and on the observation, by AFM, that the transition toward a p3 crystal is rather slow under the employed conditions, we attribute the shift in Δ of −0.24° to a complete p6 crystalline layer. Both the persistence of the purely mass-transport limited regime

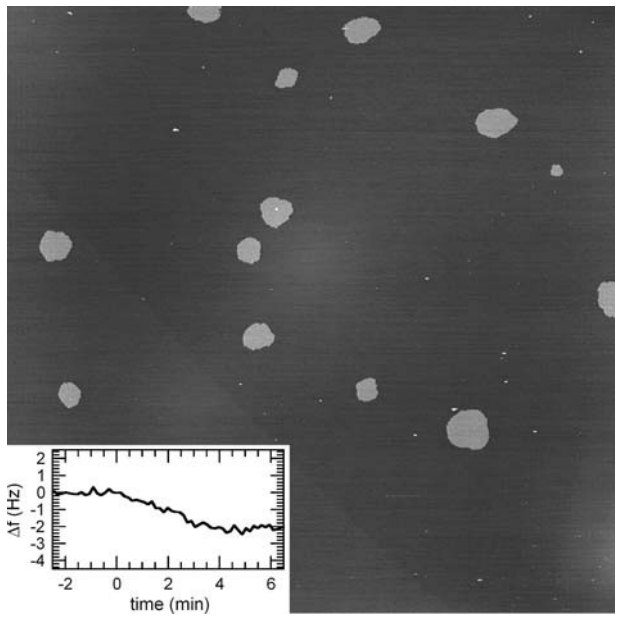

FIGURE 9 AFM images after an interrupted adsorption of annexin A5 on mica-SLBs of DOPC/DOPS (2:1); 2 μg/mL annexin A5 were incubated at 2 mM $CaCl_2$, until a coverage corresponding to a frequency shift of −2.5 Hz by QCM-D (flow mode) was reached (*inset*). The sample was rinsed in buffer containing 2 mM $CaCl_2$ (*inset*, at 4 min) before transfer to the AFM. Domains of 300 nm to 1.5 μm diameter are visible, which did not change in position or size but slightly fluctuated in shape during subsequent scans (not shown) and were identified as p6 crystalline domains. The apparent coverage with crystalline domains was ~3%. Image size (z-limit): 20 μm (10 nm).

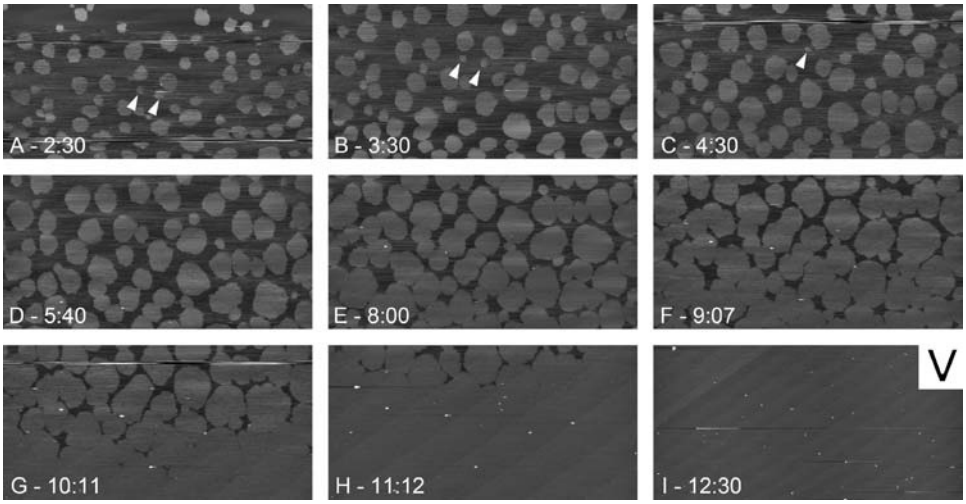

FIGURE 10 Growth of a p6 crystalline layer of annexin A5, followed in situ by AFM. Annexin A5 was injected at 20 μg/mL on mica-SLBs of DOPC/DOPS (1:2). Although most crystalline domains grow with time, a few domains (*arrowheads*) diminish in size and disappear. All images are acquired with the slow scan direction from top to bottom; the image acquisition time is ~1 min; incubation times at the end of each image are indicated (min:s). The lateral orientation of the AFM cantilever with respect to the surface is indicated schematically (*inset* in *I*). Drifts are due to instabilities in the AFM setup. Image size (z-limit): 10 × 5 μm (10 nm).

and the overall adsorption kinetics are similar on mica (Fig. 8) and on silica (Fig. 4), suggesting a rather limited influence of the crystallization on the adsorption kinetics.

When do trimer formation and 2D crystallization start?

To investigate when the crystallization of annexin A5 sets in, we followed the adsorption of annexin A5 on mica-SLBs (DOPC/DOPS (2:1)) by QCM-D and interrupted the adsorption by rinsing after a few hertz of coverage were reached (Fig. 9, *inset*). Subsequent imaging of this sample by AFM revealed small domains (Fig. 9) exhibiting the characteristic topography of a p6 crystal (not shown). Similar results were obtained on SLBs formed from DOPC/DOPS (1:2). This demonstrates that a small coverage ($\leq$10%) with annexin A5 is sufficient to initiate crystallization. In agreement, previous TEM studies on lipid monolayers (23) had reported the presence of the precursor state of trimers for very low concentrations of surface-bound annexin A5.

Kinetics of p6 crystal growth

We followed the growth of the p6 crystals by AFM in situ, after injection of annexin A5 on a preformed SLB (Fig. 10). Initially, a number of small crystalline patches appeared (Fig. 10 *A*). The smallest visible patches have a diameter of ~150 nm. Most of the patches then grow (Fig. 10, *B–H*) until they cover the entire surface (Fig. 10 *I*). It is notable that no new patches are formed after 2.5 min of incubation. Instead, a few patches (Fig. 10, *arrowheads*) were found to diminish in size before disappearing completely.

We note that the time to get to complete crystallization (~12 min in these conditions) is in the same range as the time needed for complete adsorption at similar annexin A5 concentrations (Fig. 2). A rigorous comparison of the kinetics is though not possible, as the presence of AFM tip and cantilever is susceptible to modify the mass-transport conditions for the adsorption of the protein. This is witnessed by the slightly heterogeneous crystal growth rates in Fig. 10 (e.g., compare the lower half of Fig. 10 *G* with the upper half of Fig. 10 *H*) and has already been reported elsewhere (50).

Kinetics of the p6 to p3 transition

Relatively small changes in adsorbed mass upon transition from a p6 to a p3 crystal and relatively slow kinetics rendered measurements of the transition kinetics by QCM-D or ellipsometry nonreliable. The difference in protein mass between a complete p6 and a complete p3 crystalline layer is 36 ng/cm^2, or 18% of the mass of a p6 crystalline layer, including its central trimers (34). However, both crystal forms could be clearly distinguished by AFM: at small image sizes, the differences in the crystalline structure were identified directly (Fig. 11 *A*), whereas at large image sizes, both crystalline states could be distinguished by small but detectable differences (~0.1 nm) in the crystal height (Fig. 11, *B–C*). We therefore employed AFM to follow the kinetics of the transition from a p6 to a p3 crystalline state. The observed times for the transition from a crystalline layer of pure p6 symmetry to pure p3 symmetry ranged from 10 min (e.g., for DOPC/DOPS (1:1) and 20 mM $CaCl_2$) to 60 min (e.g., for DOPC/DOPS (1:1) and 2 mM $CaCl_2$) at [A5] = 20 μg/mL. This is clearly much longer than what was commonly needed for the formation of a complete p6 crystalline layer. The slow kinetics implies that the recruitment of additional proteins from the solution is not mass-transport limited. The influence of AFM tip and cantilever on the kinetics is expected to be small in this case.

DISCUSSION

We have investigated the adsorption and 2D self-assembly of annexin A5 on silica-SLBs and on mica-SLBs. Figs. 3, 6, and 7 provide an overview of the obtained results. We find that the amount of adsorbed annexin A5 is determined by the amount

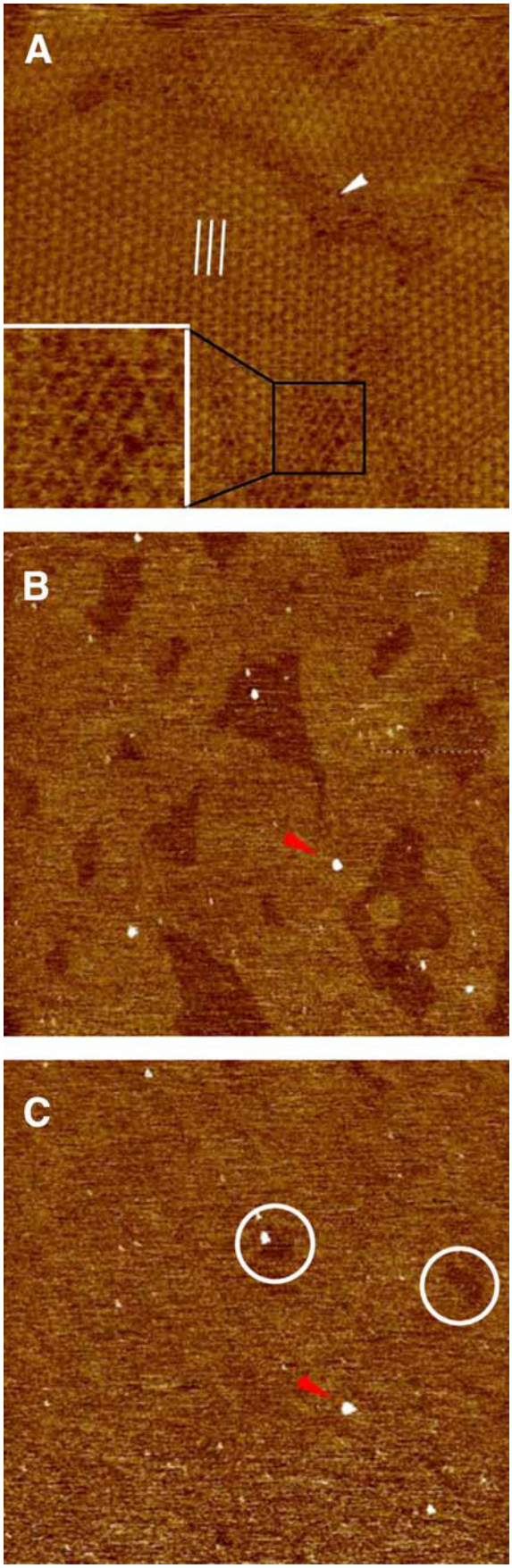

of accessible DOPS and by the concentration of calcium, which correlates well with previous work (21,26,51). The adsorption curves on silica-SLBs and mica-SLBs are highly similar, if we take into account that the accessible [DOPS] on mica-SLBs, formed from a given vesicle preparation, is significantly smaller than on silica-SLBs (38). In contrast, we find that whereas annexin A5 2D crystals of p6 symmetry readily form on mica-SLBs at low protein coverage, crystallization does not occur on silica-SLBs, except when a close-to-maximal surface coverage is reached. Our data indicate that annexin A5 can bind both to DOPS and to DOPC and we report on different regimes of reversibility of annexin A5 binding.

The interleaflet distribution of DOPS

A comment is appropriate concerning the distribution of DOPS between the two leaflets of the employed SLBs. Our previous study with prothrombin (38) provided evidence that the bulk-facing leaflet of mica-SLBs is depleted in DOPS and allowed to quantify the difference in the DOPS content in the bulk-facing leaflet of mica-SLBs relative to silica-SLBs. It remained, however, unclear whether the interleaflet distribution in silica-SLBs is symmetrical.

Our data on annexin A5 binding, obtained on silica-SLBs formed by the method of vesicle spreading and presented here, can be compared with previously reported results on SLBs formed by Langmuir-Blodgett deposition (21) and on large unilamellar vesicles (26) (c.f. Table 1). We find that the amounts of [DOPS] and [Ca] that are required for half-maximal binding of annexin A5 correlate well for all studies (c.f. Fig. 7 *A*). This indicates that the distribution of DOPS in silica-SLBs is indeed symmetrical, i.e., the nominal [DOPS] corresponds to the accessible [DOPS].

The combination of AFM, QCM-D, and ellipsometry

We emphasize that the combination of a technique with lateral resolution down to the submolecular level, such as AFM, and techniques that measure the total adsorbed amount at high time resolution, such as QCM-D or ellipsometry, was

FIGURE 11 AFM images of coexisting p6- and p3-crystalline domains of annexin A5. (*A*) The molecular organization of the p3 crystal (*white lines* follow the lattice lines) is predominant. A very small p6 domain (*black rectangle*, two times enlarged in *inset*) as well as disordered boundaries (*white arrowhead*) can be discerned; 80 μg/mL annexin A5 were incubated in 0.2 mM $CaCl_2$ on DOPC/DOPS (1:4)-SLBs before image acquisition. Image size (z-limit): 300 nm (3 nm). (*B–C*) Regions of p3 symmetry can be distinguished from regions of p6 symmetry due to slight differences (~0.1 nm) in their height, even at image sizes that prohibit molecular resolution. The images show the advancement of the p3 crystal (*lighter area*) after 34 (*B*) and 54 min (*C*) of incubation of 20 μg/mL annexin A5 in 2 mM $CaCl_2$ on DOPC/DOPS (1:2)-SLBs. In panel *C* only a few small p6 crystalline areas remain (*white circles*). A defect is marked (*red arrowhead*) for orientation. Image size (z-limit): 5 μm (1 nm).

an essential prerequisite for this study. The employed techniques proved highly complementary. AFM provided detailed information on the structure and growth of self-assembly structures, although its capability to trace adsorbed but laterally mobile molecules is limited (32) and the AFM cantilever is susceptible to affect adsorption kinetics (50). QCM-D or ellipsometry, on the other hand, give access to time-resolved information about the overall adsorbed amount, while being limited in tracing the 2D self-assembly of the protein. The unexpected observation that the 2D self-assembly of annexin A5 depends distinctly on the solid support, illustrates the importance of employing identical (in the case of mica) or similar (in the case of silica) surfaces for all techniques to obtain reliable results.

A model of annexin A5 binding

Stability of annexin A5 on SLBs

Under appropriate conditions, the adsorption of annexin A5 was observed to be completely or in part irreversible. This property of annexin A5 seems to be rather exceptional. Which mechanism can render the binding of annexin A5 so stable? Given the different states of 2D organization of membrane-bound annexin A5 one may suspect the binding stability to be enhanced by the trimerization or 2D crystallization of the protein. However, our observation that the amounts of irreversibly bound annexin A5 are very similar on mica-SLBs (that promote crystallization) and on silica-SLBs (that inhibit crystallization except at close-to-full coverage) indicates that the influence of 2D crystallization is minor. In studies to be reported elsewhere (A. R. Brisson, unpublished data), we have further investigated the stability of a number of annexin A5 mutants against desorption (on silica-SLBs containing 0, 10, and 20% DOPS). Whereas both trimerization and 2D crystallization were inhibited for these mutants, the reversibility of binding was found to be very similar to what is reported here for wild-type annexin A5. Our results thus provide evidence that the binding of annexin A5 in its monomeric state is sufficient for irreversible binding. The fact that annexin molecules consist of a fourfold repeat of a membrane-binding motif (36,52) provides a direct explanation for the irreversibility of binding of annexins' monomers.

The sigmoidal shape of the graphs in Figs. 3 and 6 indicates the presence of apparent cooperativity of annexin A5 binding to SLBs. This strongly suggests that the binding involves the calcium-mediated interaction of protein monomers with several binding sites, a scenario that was previously proposed by Meers (14).

Binding of annexin A5 to SLBs with low DOPS content

Our results at [Ca] $\leq$ 2 mM indicate that an amount of 20–25% of accessible DOPS is sufficient to generate full protein coverage. Considering the molecular areas of the lipids ($\sim$0.6 nm^2) and the protein ($\sim$30 nm^2) (26), this implies that the presence (on average) of $\sim$10 DOPS molecules per protein molecule is required for full and completely irreversible binding. This does not mean that all molecules are bound to the protein.

At DOPS concentrations below 20% the surface environment provided by the membrane is not sufficient to generate fully irreversible binding. In this case, the distribution of lipid molecules may be such that the local membrane environment that is required for irreversible binding and determined by the presence of DOPS, DOPC, and calcium, is not attained homogeneously over the entire surface. This may explain our finding that a small population of reversibly bound proteins coexists with another population of irreversibly bound annexin A5 under conditions of incomplete coverage (c.f. Figs. 3 and 6).

The presence of two different protein populations, one reversibly and the other irreversibly bound, has previously been reported by Kastl et al. (53) for annexin A1. The authors proposed this phenomenon to originate from the formation of PS-enriched membrane domains and self-association of the protein molecules. However, the 2D assembly of annexin A5 did not markedly influence its binding stability, as described above. In some cases, we found slightly increased amounts of reversibly bound annexin A5 on mica-SLBs as compared to silica-SLBs. Under these particular conditions the incorporation of annexin A5 into a crystal may act as a secondary binding transition that enhances the apparent binding affinity of annexin A5. Furthermore, we observed partly irreversible binding on SLBs of pure DOPC (discussed below), indicating that the formation of membrane domains is not necessary to produce two different populations of the bound protein.

Taken together we propose that the adsorption of annexin A5 is determined by the interaction of protein monomers with the local membrane environment. The membrane environment, as defined by the presence of DOPS, DOPC, and calcium ions, controls the adsorption and reversibility of binding. We emphasize that the model in its simplest form does not require any assumptions about specific interlipid or interprotein interactions, such as the formation of nanoscopic lipid domains or the oligomerization of annexin A5. In particular, we note that these results invalidate an earlier model in which a minimal number of DOPS molecules, inferior to the number of bound annexin A5 molecules, was considered sufficient to act as anchoring points for the annexin A5 2D ordered assembly (26).

Binding of annexin A5 to DOPC

We found that annexin A5 also adsorbs to pure DOPC membranes, in agreement with previous studies (21,23). What are the differences in binding of annexin A5 to pure DOPC membranes as compared to DOPS-rich membranes? Firstly, calcium concentrations of 20 mM and more are required for

binding to DOPC, whereas concentrations of 0.1–1 mM are sufficient for DOPS-rich membranes. Secondly, we observed differences in the reversibility of binding. Binding to DOPC is completely reversible at 20 mM $CaCl_2$ with half-maximal binding occurring at ~40 mg/mL of annexin A5. We could not find such a regime on DOPS-rich membranes. One may suggest that a regime of extensive, but fully reversible adsorption may exist for DOPS-rich SLBs at a calcium concentration between 20 and 200 mM (which is not covered by the presented experimental data). We checked this for an SLB containing 25% DOPS and could not find such a regime. Binding to DOPC can though be irreversible, at least in part, as demonstrated for 200 mM $CaCl_2$.

Our results may suggest that the molecular mechanisms by which annexin A5 interacts with DOPC and DOPS, respectively, are different. An alternative view that appears to be relevant in light of our results has been proposed by Meers (14). Motivated by observations on micellar systems, Meers suggested that the intrinsic interaction of annexin A5 with molecules of DOPC and DOPS, respectively, may be identical. In the framework of his scenario, differences in the apparent adsorption behavior are due to the charge of DOPS that increases the concentration of calcium ions in the vicinity of the membrane and thereby increases protein binding. Our data can neither fully support nor fully refute one of the two scenarios. However, the observed differences in reversibility of binding indicate that, in Meers' scenario, the role of the lipid charge must go beyond the simple enrichment of the membrane surface in calcium.

Kinetics of annexin A5 2D crystallization on mica-SLBs

The principal phases and phase transitions in the 2D self-assembly of annexin A5 on mica-SLBs have been investigated in previous studies (5,23) (Fig. 1). In comparison to these reports we have extended the range of employed DOPS concentrations (including pure DOPC) and calcium concentrations (0–200 mM). We find that the previously outlined phases and phase transitions apply over the entire range of investigated concentrations of DOPS and calcium: at low protein coverage the p6 crystalline form is observed exclusively, whereas p3 crystals occur only once the state of complete coverage with a p6 crystal has been surpassed. Fig. 7 demonstrates that the propensity to form p6 and p3 crystals is generally determined by the concentration of [DOPS] and [Ca]. For a given [Ca], a critical concentration of [DOPS] exists above which the transition to the p3 crystal form can occur.

Nucleation and growth of p6 crystals

The fact that stable 2D crystals of annexin A5 were found at a protein coverage that corresponds to a small fraction of the maximum coverage (c.f. Fig. 9) provides evidence that a low 2D protein density ($\leq$10%) is sufficient to initiate nucleation and growth of p6 crystals.

Under the experimental conditions employed, the time window for crystal nucleation is small (c.f. Fig. 10). No new crystalline domains appear shortly after the formation of the first domains. This suggests that the growth of existing crystals keeps the density of adsorbed noncrystalline proteins sufficiently low to prevent further nucleation. Some crystallites actually diminish in size and disappear (c.f. Fig. 10), which may be indicative of Ostwald ripening. Thus, protein adsorption is expected to limit crystal growth, which is consistent with our findings: i), that adsorption is mass-transport limited up to high coverage and reaches equilibrium quickly, as well as ii), that crystallization rates and adsorption rates are similar.

Our observation that crystallization starts at low protein coverage and exhibits high growth rates confirms that the formation of trimers, the precursor of crystallization, is fast and occurs at a very low density of membrane-bound proteins, as previously reported on vesicles (for annexin A12, another member of the annexin family that exhibits strong similarities to annexin A5 in its membrane binding properties) (54) and on lipid monolayers (23).

The transition from p6 to p3

The solid-solid phase transition from the p6 to the denser p3 crystal form is of first order (5); p3 nuclei form at the grain boundaries or in defects of the p6 crystallites and grow by the adsorption of additional annexin A5 molecules into surface areas that are liberated due to the higher density (~17%) of the p3 crystal form as compared to the p6 crystal form. The membrane surface available for binding is thus determined by the local fluctuations in the crystalline state and is generally expected to be small. Consequently, the adsorption in this regime is strongly limited by surface-blocking effects, consistent with our finding that the growth of p3 crystals is generally slower than the growth of p6 crystals. In addition to these surface-blocking effects, the density of available binding sites, as determined by [DOPS] and [Ca], is expected to restrict the rates of adsorption and p3 crystal growth. This rationalizes our observation that the p3 crystallization rate increases with increasing [DOPS] and [Ca].

Annexin A5 2D assembly on silica-SLBs

We have provided evidence that the p6 crystal form is not present on silica-SLBs, in strong contrast to mica-SLBs. This result came as a surprise because the properties of the bulk-facing SLB leaflet are commonly expected to be fairly independent on the properties of the underlying support. In fact, we observed ordered structures of annexin A5 at high protein coverage, which clearly demonstrates that annexin A5 2D ordered assemblies can be formed on silica-SLBs.

On the other hand, the mechanical stability of annexin A5 p6 crystals is limited (55). For example, mechanical stress exerted upon transfer of p6 crystals—formed on lipid monolayers at the air-water interface—to electron microscopy grids coated with continuous carbon films induced their transition into the p3 crystal form (17). Similarly, differences in the properties of the solid support (roughness, crystallinity) (32) may induce slight changes in the SLB properties (lipid mobility) that render the p6 crystalline form unfavorable as compared to the disordered state of annexin A5 trimers. Further studies on similar surfaces such as crystalline silica or glass may reveal more insight, but are outside the scope of this work.

CONCLUSION AND PERSPECTIVES

We have provided a detailed characterization of the binding and 2D self-assembly of annexin A5 on SLBs for a large range of calcium concentrations and DOPS contents, including pure DOPC. The combination of AFM, QCM-D, and ellipsometry allowed correlating the kinetics of adsorption and 2D crystallization.

We found that the adsorption of annexin A5 is determined by the interaction of protein monomers with the membrane and propose that the local membrane environment, as defined by the presence of DOPC, DOPS, and calcium ions, controls the adsorption and reversibility of binding.

We found genuine differences in the self-assembly behavior of annexin A5 on SLBs formed on silica and mica, respectively. Whereas the origin of these differences remains unclear, our results stress that the solid support can have a pronounced influence on the properties of SLBs.

Although we have predominantly treated the 2D crystallization kinetics in a qualitative manner, the outlined experimental approaches are expected to be useful for the quantitative characterization of the 2D self-assembly process (3).

We thank Wim Hermens (University of Maastricht, Maastricht, The Netherlands) for providing access to the ellipsometer as well as Aleš Benda and Martin Beneš (Heyrovský Institute, Prague, Czech Republic) for help with its setup. Furthermore, we thank Patrice Caillat and Claude Vauchier (CEA-LETI, Grenoble, France) for the gift of silicon wafers. We acknowledge discussions with Ilya Reviakine (University of Clausthal, Clausthal-Zellerfeld, Germany).

Ralf Richter was supported by the Conseil Régional d'Aquitaine (France) and by European Community grant FP6-NMP4-CT2003-505868 ''Nanocues''. This research was supported by the Conseil Régional d'Aquitaine, the Fonds Européen de Développement Régional, and European Community grant FP6-NMP4-CT2003-505868 ''Nanocues''.

REFERENCES

1. McPherson, A. 2003. Macromolecular crystallization in the structural genomics area. *J. Struct. Biol.* 142:1–2.
2. Nogales, E., S. G. Wolf, and K. H. Downing. 1998. Structure of the alpha beta tubulin dimer by electron crystallography. *Nature*. 391: 199–203.
3. Doudevski, I., W. A. Hayes, and D. K. Schwartz. 1998. Submonolayer island nucleation and growth kinetics during self-assembled monolayer formation. *Phys. Rev. Lett.* 81:4927–4930.
4. Giegé, R., and A. Ducruix. 1999. Crystallization of Nucleic Acids and Proteins: A Practical Approach. A. Ducruix and R. Giegé, editors. Oxford University Press, Oxford, UK.
5. Reviakine, I., A. Bergsma-Schutter, A. N. Morozov, and A. Brisson. 2001. Two-dimensional crystallization of annexin A5 on phospholipid bilayers and monolayers: a solid-solid phase transition between crystal forms. *Langmuir*. 17:1680–1686.
6. Farah, S. J., S.-W. Wang, W.-H. Chang, C. R. Robertson, and A. P. Gast. 2001. Point mutagenesis and cocrystallization of wild-type and mutant proteins: a study of solid-phase coexistence in two-dimensional protein arrays. *Langmuir*. 17:5731–5735.
7. Chernov, A. A. 2003. Protein crystals and their growth. *J. Struct. Biol.* 142:3–21.
8. Hemming, S. A., A. Bochkarev, S. A. Darst, R. D. Kornberg, P. Ala, D. S. C. Yang, and A. M. Edwards. 1995. The mechanism of protein crystal growth from lipid layers. *J. Mol. Biol.* 246:308–316.
9. Malkin, A. J., Y. G. Kuznetsov, T. A. Land, J. J. DeYoreo, and A. McPherson. 1995. Mechanisms of growth for protein and virus crystals. *Nat. Struct. Biol.* 2:956–959.
10. Strandburg, K. J. 1988. Two-dimensional melting. *Rev. Mod. Phys.* 60:161–207.
11. Oesterhelt, D., and W. Stoeckenius. 1971. Rhodopsin-like protein from the purple membrane of Halobacterium halobium. *Nat. New Biol.* 233:149–152.
12. Müller, D. J., C.-A. Schoenenberger, F. Schabert, and A. Engel. 1997. Structural changes in native membrane proteins monitored at subnanometer resolution with the atomic force microscope: a review. *J. Struct. Biol.* 119:149–157.
13. Ratanabanangkoon, P., and A. P. Gast. 2003. Effect of ionic strength on two-dimensional streptavidin crystallization. *Langmuir*. 19:1794–1801.
14. Meers, P. 1996. Annexin binding to lipid assemblies. *In* Annexins: Molecular Structure to Cellular Function. B. A. Seaton, editor. R. G. Landes Company, Austin, TX. 97–119.
15. Mosser, G., C. Ravanat, J.-M. Freyssinet, and A. Brisson. 1991. Subdomain structure of lipid-bound annexin-V resolved by electron image analysis. *J. Mol. Biol.* 217:241–245.
16. Voges, D., R. Berendes, A. Burger, P. Demange, W. Baumeister, and R. Huber. 1994. Three-dimensional structure of membrane-bound annexin V: a correlative electron microscopy-X-ray crystallography study. *J. Mol. Biol.* 238:199–213.
17. Brisson, A., A. Bergsma-Schutter, F. Oling, O. Lambert, and I. Reviakine. 1999. Two-dimensional crystallization of proteins on lipid monolayers at the air-water interface and transfer to an electron microscopy grid. *J. Cryst. Growth*. 196:456–470.
18. Oling, F., W. Bergsma-Schutter, and A. Brisson. 2001. Trimers, dimers of trimers, and trimers of trimers are common building blocks of annexin A5 two-dimensional crystals. *J. Struct. Biol.* 133: 55–63.
19. Reviakine, I., W. Bergsma-Schutter, and A. Brisson. 1998. Growth of protein 2-D crystals on supported planar lipid bilayers imaged in situ by AFM. *J. Struct. Biol.* 121:356–361.
20. Oling, F., J. Sopkova-de Oliveira Santos, N. Govorukhina, C. Mazères-Dubut, W. Bergsma-Schutter, G. Oostergetel, W. Keegstra, O. Lambert, A. Lewit-Bentley, and A. Brisson. 2000. Structure of membrane-bound annexin A5 trimers: a hybrid cryo-EM-X-ray crystallography study. *J. Mol. Biol.* 304:561–573.
21. Andree, H. A. M., C. P. M. Reutelingsperger, R. Hauptmann, H. C. Hemker, W. T. Hermens, and G. M. Willems. 1990. Binding of

vascular anticoagulant α (VACα) to planar phospholipid bilayers. *J. Biol. Chem.* 265:4923–4928.

22. Andree, H. A. M., M. C. A. Stuart, W. T. Hermens, C. P. M. Reutelingsperger, H. C. Hemker, P. M. Frederik, and G. M. Willems. 1992. Clustering of lipid-bound annexin V may explain its anticoagulant effect. *J. Biol. Chem.* 267:17907–17912.
23. Govorukhina, N., A. Bergsma-Schutter, C. Mazères-Dubut, S. Mazères, E. Drakopoulou, L. Bystrykh, F. Oling, A. Mukhopadhyay, I. Reviakine, J. Lai Kee Him, and A. Brisson. 2003. Self-assembly of annexin A5 on lipid membranes. *In* Annexins: Biological Importance and Annexin-Related Pathologies. J. Bandorowicz-Pikula, editor. Landes Bioscience/Eurekah.com, Georgetown, TX. 37–55.
24. Meers, P. 1990. Location of tryptophans in membrane-bound annexins. *Biochemistry.* 29:3325–3330.
25. Meers, P., and T. Mealy. 1993. Relationship between annexin V tryptophan exposure, calcium, and phospholipid binding. *Biochemistry.* 32: 5411–5418.
26. Pigault, C., A. Follenius-Wund, M. Schmutz, J.-M. Freyssinet, and A. Brisson. 1994. Formation of two-dimensional arrays of annexin V on phosphatidylserine-containing liposomes. *J. Mol. Biol.* 236: 199–208.
27. Tait, J. F., D. Gibson, and K. Fujikawa. 1989. Phospholipid binding properties of human placental anticoagulant protein-I a member of the lipocortin family. *J. Biol. Chem.* 264:7944–7949.
28. Blackwood, R. A., and J. D. Ernst. 1990. Characterization of Ca^{2+}-dependent phospholipid binding vesicle aggregation and membrane fusion by annexins. *Biochem. J.* 266:195–200.
29. Brisson, A., G. Mosser, and R. Huber. 1991. Structure of soluble and membrane-bound human annexin V. *J. Mol. Biol.* 220:199–203.
30. Reviakine, I., W. Bergsma-Schutter, C. Mazères-Dubut, N. Govorukhina, and A. Brisson. 2000. Surface topography of the p3 and p6 annexin V crystal forms determined by atomic force microscopy. *J. Struct. Biol.* 131:234–239.
31. Noro, M. G., M. A. Bates, A. Brisson, and D. Frenkel. 2002. Modeling the phase behavior of the membrane binding protein annexin V. *Langmuir.* 18:2988–2992.
32. Richter, R. P., and A. Brisson. 2003. Characterization of lipid bilayers and protein assemblies supported on rough surfaces by atomic force microscopy. *Langmuir.* 19:1632–1640.
33. Richter, R. P., A. Mukhopadhay, and A. Brisson. 2003. Pathways of lipid vesicle deposition on solid surfaces: a combined QCM-D and AFM study. *Biophys. J.* 85:3035–3047.
34. Richter, R. P., and A. Brisson. 2004. QCM-D on mica for parallel QCM-D: AFM studies. *Langmuir.* 20:4609–4613.
35. Richter, R. P., and A. Brisson. 2005. Following the formation of supported lipid bilayers on mica: a study combining AFM, QCM-D, and ellipsometry. *Biophys. J.* 88:3422–3433.
36. Pepinsky, R. B., R. Tizard, R. J. Mattaliano, L. K. Sinclair, G. T. Miller, J. L. Browning, E. P. Chow, C. Burne, K. S. Huang, D. Pratt, L. Wachter, C. Hession, A. Frey, and B. Wallner. 1988. Five distinct calcium and phospholipid binding proteins share homology with lipocortin I. *J. Biol. Chem.* 263:10799–10811.
37. Rodahl, M., F. Höök, A. Krozer, P. Brzezinski, and B. Kasemo. 1995. Quartz crystal microbalance setup for frequency and Q-factor measurements in gaseous and liquid environments. *Rev. Sci. Instrum.* 66:3924–3930.
38. Richter, R. P., N. Maury, and A. Brisson. 2005. On the effect of the solid support on the inter-leaflet distribution of lipids in supported lipid bilayers. *Langmuir.* 21:299–304.
39. Sauerbrey, G. 1959. Verwendung von Schwingquartzen zur Wägung dünner Schichten und zur Mikrowägung. [in German]. *Z. Phys.* 155:206–222.
40. Cuypers, P. A., J. W. Corsel, M. P. Janssen, J. M. M. Kop, W. T. Hermens, and H. C. Hemker. 1983. The adsorption of prothrombin to phosphatidylserine multilayers quantitated by ellipsometry. *J. Biol. Chem.* 258:2426–2430.
41. Tompkins, H. G. 1993. A User's Guide to Ellipsometry. Academic Press, London, UK.
42. Corsel, J. W., G. M. Willems, J. M. M. Kop, P. A. Cuypers, and W. T. Hermens. 1986. The role of intrinsic binding rate and transport rate in the adsorption of prothrombin, albumin and fibrinogen to phospholipid bilayers. *J. Colloid Interface Sci.* 111:544–554.
43. Benes, M., D. Billy, A. Benda, H. Speijer, M. Hof, and W. T. Hermens. 2004. Surface-dependent transitions during self-assembly of phospholipid membranes on mica, silica, and glass. *Langmuir.* 20:10129–10137.
44. Benes, M., D. Billy, W. T. Hermens, and M. Hof. 2002. Muscovite (mica) allows the characterization of supported bilayers by ellipsometry and confocal fluorescence correlation spectroscopy. *Biol. Chem.* 383:337–341.
45. Hermens, W. T., M. Benes, R. P. Richter, and H. Speijer. 2004. Effects of flow on solute exchange between fluids and supported biosurfaces. An overview. *Biotechnol. Appl. Biochem.* 39:277–284.
46. Keller, C. A., and B. Kasemo. 1998. Surface specific kinetics of lipid vesicle adsorption measured with a quartz crystal microbalance. *Biophys. J.* 75:1397–1402.
47. Reimhult, E., F. Höök, and B. Kasemo. 2002. Vesicle adsorption on SiO_2 and TiO_2: dependence on vesicle size. *J. Chem. Phys.* 117:7401–7404.
48. Rädler, J., M. Radmacher, and H. E. Gaub. 1994. Velocity-dependent forces in atomic force microscopy imaging of lipid films. *Langmuir.* 10:3111–3115.
49. Saffman, P. G., and M. Delbrück. 1975. Brownian motion in biological membranes. *Proc. Natl. Acad. Sci. USA.* 72:3111–3113.
50. Leitner, T., G. Friedbacher, T. Vallant, H. Brunner, U. Mayer, and H. Hoffmann. 2000. Investigations of the growth of self-assembled octadecylsiloxane monolayers with atomic force microscopy. *Mikrochim. Acta.* 133:331–336.
51. Andree, H. A. M. 1992. Phospholipid binding and anticoagulant action of annexin V. PhD thesis. University of Maastricht, Maastricht, The Netherlands.
52. Huber, R., J. M. Römisch, and E. P. Paques. 1990. The crystal and molecular structure of human annexin V, an anticoagulant protein that binds to calcium and membranes. *EMBO J.* 9:3867–3874.
53. Kastl, K., A. Herrig, E. Lüthgens, A. Janshoff, and C. Steinem. 2004. Scrutiny of annexin A1 mediated membrane-membrane interaction by means of a thickness shear mode resonator and computer simulations. *Langmuir.* 20:7246–7253.
54. Langen, R., J. M. Isas, H. Luecke, H. T. Haigler, and W. L. Hubbell. 1998. Membrane-mediated assembly of annexins studied by site-directed spin labeling. *J. Biol. Chem.* 273:22453–22457.
55. Vénien-Bryan, C., P.-F. Lenne, C. Zakri, A. Renault, A. Brisson, J.-F. Legrand, and B. Berge. 1998. Characterization of the growth of 2D protein crystals on a lipid monolayer by ellipsometry and rigidity measurements coupled to electron microscopy. *Biophys. J.* 74:2649–2657.